Highly resolved infrared spectra of pure CO_2 ice (15–75 K)[*]

K. Isokoski[1], C. A. Poteet[2,3], and H. Linnartz[1]

[1] Raymond and Beverly Sackler Laboratory for Astrophysics, Leiden Observatory, Leiden University, PO Box 9513, 2300 RA Leiden, The Netherlands
e-mail: isokoski@strw.leidenuniv.nl
[2] Department of Physics and Astronomy, The University of Toledo, 2801 West Bancroft Street, Toledo, OH 43606, USA
[3] Current address: New York Center for Astrobiology, Rensselaer Polytechnic Institute, 110 Eighth Street, Troy, NY 12180, USA

ABSTRACT

Context. The ν_2 bending mode of pure CO_2 ice around 15.2 μm exhibits a fine double-peak structure that offers a sensitive probe to study the physical and chemical properties of solid CO_2 in space. Current laboratory spectra do not fully resolve the CO_2 ice features.
Aims. To improve the fitting of the observed CO_2 features, high-resolution solid-state infrared spectra of pure CO_2 ice are recorded in the laboratory for a series of astronomically relevant temperatures and at an unprecedented level of detail.
Methods. The infrared spectra of pure CO_2 ice were recorded in the 4000 to 400 cm^{-1} (2.5–25 μm) region at a resolution of 0.1 cm^{-1} using Fourier transform infrared spectroscopy.
Results. Accurate band positions and band widths (FWHM) of pure CO_2 ice are presented for temperatures of 15, 30, 45, 60, and 75 K. The focus of this spectroscopic work is on the CO_2 (ν_2) bending mode, but more accurate data are also reported for the $^{12}CO_2$ and $^{13}CO_2$ (ν_3) stretching mode, and CO_2 ($\nu_1+\nu_3$) and ($2\nu_2+\nu_3$) combination bands.

Key words. astrochemistry – line: profiles – methods: laboratory – techniques: spectroscopic – ISM: lines and bands – ISM: molecules

1. Introduction

Solid carbon dioxide, CO_2, is an important tracer of the chemical and physical history of protostars and their surroundings (Whittet et al. 1998; Ehrenfreund et al. 1998; Gerakines et al. 1999; Boogert et al. 2000; Nummelin et al. 2001; Pontoppidan et al. 2008). It constitutes a significant part of interstellar ice with abundances relative to solid H_2O varying from ~15 to 40% in quiescent dark clouds (d'Hendecourt & Jourdain de Muizon 1989; Whittet et al. 1998, 2007, 2009; Bergin et al. 2005; Knez et al. 2005) and circumstellar envelopes of low- and high-mass protostars (Gerakines et al. 1999; Nummelin et al. 2001; Boogert et al. 2004; Pontoppidan et al. 2008; Zasowski et al. 2009; Cook et al. 2011). Also in planetary environments CO_2 ice has been detected (see e.g., Cruikshank et al. 2010). The observed abundances of solid CO_2 in the interstellar medium (ISM) are a factor of ~100 higher than in the gas phase (van Dishoeck et al. 1996; Boonman et al. 2003) and cannot be reproduced by gas-phase chemical models (Bergin et al. 1995). The formation of CO_2 is therefore assumed to proceed through reactions in ices on interstellar dust grains.

CO_2 is readily produced in UV photoprocessed CO-H_2O laboratory ice, with an efficiency high enough to be driven by the cosmic-ray induced UV field in dense interstellar regions (Watanabe & Kouchi 2002). Comparable CO_2 ice abundances are however observed in regions with and without additional UV photons from a nearby protostar, suggesting a formation route which does not depend critically on the available UV field. Cosmic-ray processing of pure CO laboratory ice has been also

shown to be a viable mechanism for CO_2 production in the ISM (Jamieson et al. 2006), and seems plausible given the large abundances of pure CO ice (Pontoppidan et al. 2003). A number of other reaction schemes have been proposed and/or studied including nonenergetic surface-catalyzed CO oxidation (Tielens & Hagen 1982; Roser et al. 2001; Madzunkov et al. 2006; Raut & Baragiola 2011; Talbi et al. 2006; Slanger et al. 1972; Goumans & Andersson 2010); hydrogenation of CO-O_2 binary ice, providing a formation route through the CO-OH intermediate (Ioppolo et al. 2011); and energetic processing (photon and ion irradiation) of ices containing C- and O-bearing molecules as well as carbon grains covered by water ice (Moore et al. 1991; Gerakines et al. 1996; Palumbo et al. 1998; Satorre et al. 2000; Mennella et al. 2004; Loeffler et al. 2005; Gomis & Strazzulla 2005; Mennella et al. 2006; Ioppolo et al. 2009; Fulvio et al. 2012). Recent observational and experimental work suggests that interstellar ices are unlikely to contain significant amounts of CO intimately mixed in H_2O (Pontoppidan et al. 2003; Cuppen et al. 2011). This is inconsistent with the CO_2 formation mechanisms relying on or resulting from CO in H_2O-rich ices. Cuppen et al. (2011) further demonstrated that the astronomically observed CO ice feature is better reproduced by CO mixed in CH_3OH ice. Indeed, CH_3OH is readily produced through CO hydrogenation (Watanabe et al. 2004, 2006; Fuchs et al. 2009) and CO_2 produced in water-poor CO ice should therefore be intimately mixed also with CH_3OH.

The molecular environment in which CO_2 is observed provides, therefore, valuable information on its formation mechanism; CO_2 located in ice dominated by H_2O, CO and/or CH_3OH is a direct hint for a possible chemical connection. The CO_2 (ν_2) bending mode at 15.2 μm (660 cm^{-1}) is particularly sensitive to its molecular environment and has been observed

toward a number of sources ranging from luminous young stars (Gerakines et al. 1999; Pontoppidan et al. 2008) to cold, quiescent molecular clouds (Knez et al. 2005; Bergin et al. 2005; Whittet et al. 2007). The appearance of absorption features not only depends on ice composition, but also on ice temperature. To characterize different ice environments, the observed CO_2 (ν_2) feature can be decomposed phenomenologically into a finite set of known laboratory ice compositions (Pontoppidan et al. 2008) including pure CO_2 ice. While the profile of the CO_2 feature in each component is fixed, the relative contribution varies from source to source, thus characterizing and quantifying the ices along the line of sights.

A large number of laboratory spectra of solid CO_2 in different molecular environments and for different temperatures are available (Sandford & Allamandola 1990; Ehrenfreund et al. 1997, 1999; van Broekhuizen et al. 2006; White et al. 2009, 2012). For most sources, the analysis of the CO_2 (ν_2) feature implies the presence of both hydrogen-rich ($H_2O:CO_2$) and hydrogen-poor ($CO:CO_2$) CO_2 ice, as well as CH_3OH containing CO_2 ice (Ehrenfreund et al. 1998), consistent with several of the proposed formation schemes. Most sources also exhibit some contribution from pure CO_2 ice. The occurrence of pure CO_2 ice is considered to be a result of thermal processing, which causes segregation and/or distillation of mixed components with different volatility (Ehrenfreund et al. 1998; Öberg et al. 2009; Fayolle et al. 2011). Distillation of CO-rich ice happens at 20–30 K (van Broekhuizen et al. 2006; Pontoppidan et al. 2008). In the laboratory, segregation from H_2O-rich ice requires strong (>100 K) heating (Gerakines et al. 1999), but is lowered to 30 K in the ISM due to longer time scales (Öberg et al. 2009).

Low-temperature (<20 K) H_2O- and CO-rich ices are characterized by a broad single-peaked CO_2 (ν_2) feature, whereas pure CO_2 produces a double-peaked substructure (Ehrenfreund et al. 1997; van Broekhuizen et al. 2006). In a pure CO_2 lattice the axial symmetry of the linear molecule is broken, giving rise to the so-called Davydov splitting (Davydov 1962; Tso & Lee 1985). The splitting makes the CO_2 bending mode a sensitive probe for the changes in its environment. Prior to this work, the available laboratory spectra of pure CO_2 ice (Sandford & Allamandola 1990; Hudgins et al. 1993; Ehrenfreund et al. 1997; Baratta & Palumbo 1998) were recorded at resolutions of 1–2 cm^{-1}, too low to fully resolve the CO_2 (ν_2) bending mode. van Broekhuizen et al. (2006) recorded CO_2 ice spectra at 15–90 K with 0.5 cm^{-1} resolution but the low signal-to-noise ratio (S/N) prohibited an accurate comparison with astronomical data. Particularly for sources with a prominent double-peak structure, such as HOPS-68 (Poteet et al. 2011, 2013), the spectral quality of the used pure CO_2 component is important. Using a pure CO_2 component with a properly resolved Davydov splitting can help to avoid overestimation and misinterpretation of the underlying broader features. Ehrenfreund et al. (1997) did not make available the entire temperature series for pure CO_2 ice. Here we present a complete, high-resolution temperature series. In addition to the 15.2 μm bending mode, the resolution of the previous data is not sufficient when studying the narrow (ν_3) $^{13}CO_2$ or ($\nu_1+\nu_3$) CO_2 combination ice bands. These bands are studied here as well and will be accessible with the *James Webb* Space Telescope.

2. Experimental procedure

The experiments are performed in a high-vacuum (HV) setup first described by Gerakines et al. (1995) (Fig. 1). A stainless
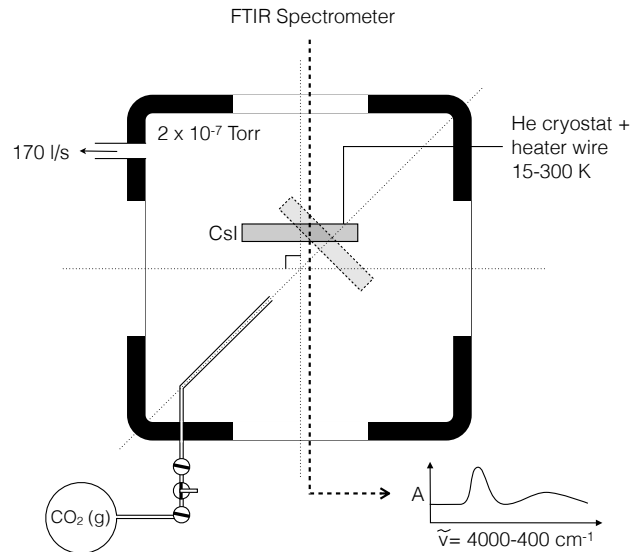
Fig. 1. Schematic drawing of the experimental setup for preparation and spectroscopic characterization of the cryogenic CO_2 samples.

steel chamber is evacuated by a turbomolecular pump (170 l s^{-1}; Pfeiffer TPH 170) and a rotary vane pump (6 m^3 h^{-1}; Edwards E2M8) separated by an oil mist filter, allowing a base pressure of 2.5×10^{-7} mbar at room temperature. The chamber houses a CsI (Caesium Iodide) sample substrate that is cooled down to 15 K by a closed cycle helium cryostat (ADP DE-202). The substrate temperature is controlled between 15 and 300 K, with a precision of 0.1 K, by a resistive heater element and a silicon diode sensor using an external temperature control unit (LakeShore 330). CO_2 (Praxair, 99.998% purity) is introduced into the system from a gas bulb at 10 mbar filled in a separate vacuum manifold (base pressure ~10^{-5} mbar). CO_2 ices are grown onto the substrate at 15 K via effusive dosing of the gaseous sample through a stainless steel capillary along the surface normal. The approximate growth rate is determined by setting the exposure to ~10^{16} molecules cm^{-2} s^{-1}. Assuming a monolayer surface coverage of 10^{15} molecules cm^{-2} and a sticking probability of 1, this results in a growth rate of 10 L s^{-1} [1]. Ices are deposited for 5 min resulting in approximately ~3000 ML. The exact thickness of the samples is derived from the IR band strengths (Sect. 4).

The ices are heated from 15 K to 30, 45, 60, 75 and 90 K at a rate of 2 K min^{-1} and allowed to relax for 5 min before recording the absorption spectra. A Fourier transform infrared (FTIR) spectrometer (Varian 670-IR) is used to record the ice spectra in transmission mode from 4000 to 400 cm^{-1} (2.5–25 μm) with a spectral resolution of 0.1 cm^{-1}, averaging a total of 256 scans to increase the S/N. Background spectra are acquired at 15 K prior to deposition and subtracted from the recorded ice spectra. The spectra recorded at different temperatures correspond to different ice samples prepared under identical conditions. This procedure is used to minimize sample contamination during the relatively long acquisition time (~2 h).

3. Results

Figures 2–5 show the high-resolution (0.1 cm^{-1}) FTIR spectra of CO_2 ice at 15, 30, 45, 60 and 75 K. The separate graphs are offset for clarity. Figure 2 shows the spectral region around the ν_2

---

[1]   1 L (Langmuir) = 1×10^{-6} Torr s $\approx$ 1 ML.
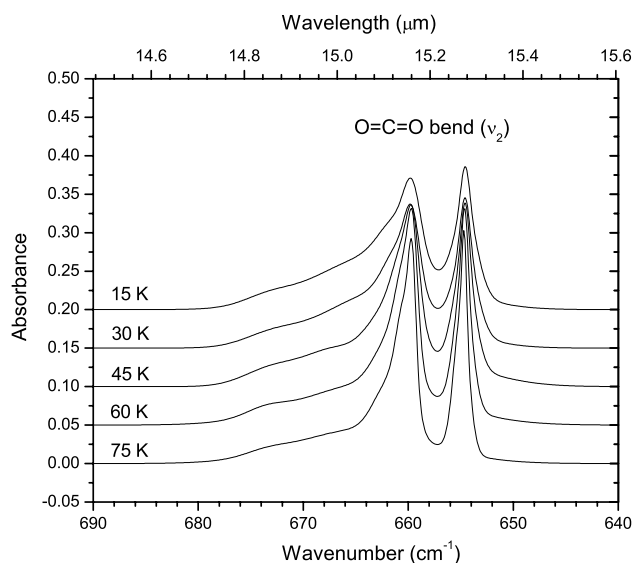
Fig. 2. High-resolution (0.1 cm^{-1}) solid-state IR spectra of pure CO$_2$ ice at 15–75 K showing the ^{12}CO$_2$ (ν_2) bending mode. The displayed spectra are obtained by smoothing through superposition of Gaussians.
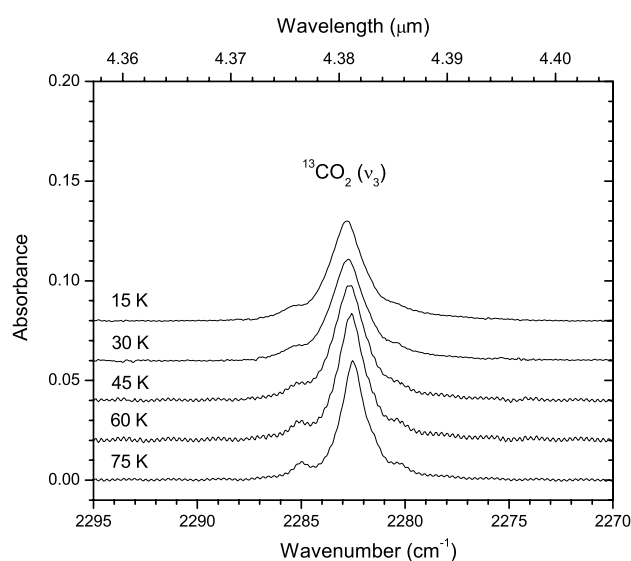
Fig. 4. High-resolution (0.1 cm^{-1}) solid-state IR spectra of pure CO$_2$ ice at 15–75 K showing the ^{13}CO$_2$ (ν_3) stretching mode. The displayed spectra are baseline corrected.
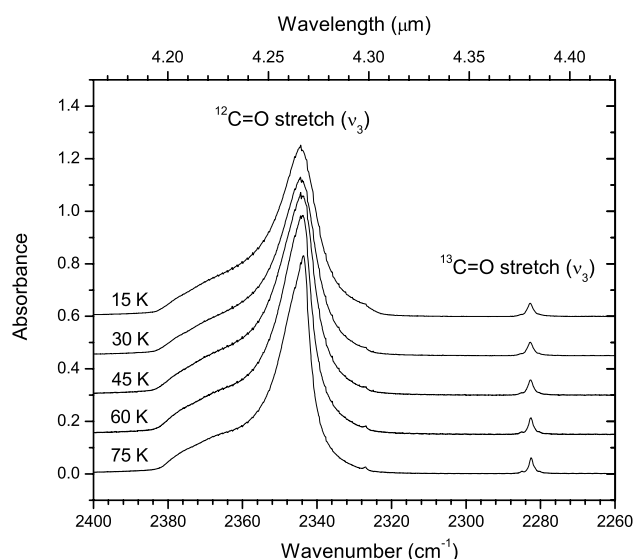
Fig. 3. High-resolution (0.1 cm^{-1}) solid-state IR spectra of pure CO$_2$ ice at 15–75 K showing the ^{12}CO$_2$ and ^{13}CO$_2$ (ν_3) stretching modes. The zoom-in of the latter is shown in Fig. 4. The displayed spectra are baseline corrected. Gaseous CO$_2$ absorption features have been subtracted.
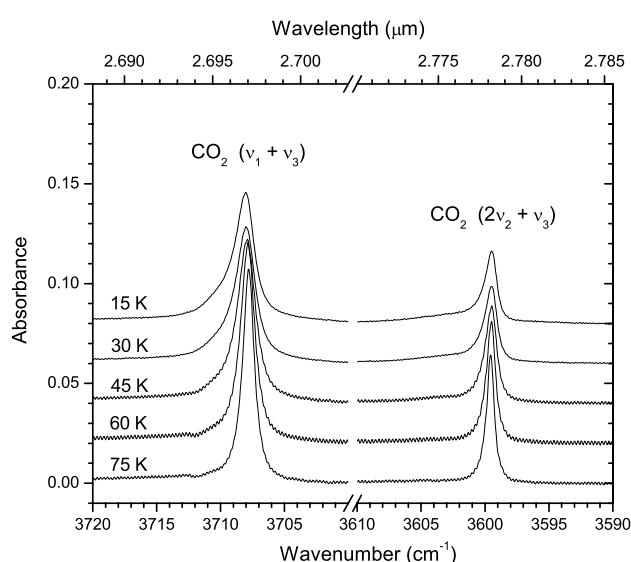
Fig. 5. High-resolution (0.1 cm^{-1}) solid-state IR spectra of pure CO$_2$ ice at 15–75 K showing the ($\nu_1 + \nu_3$) and ($2\nu_2 + \nu_3$) combination bands. The displayed spectra are baseline corrected.

bending mode (680–645 cm^{-1}). Figures 3 and 4 show the CO$_2$ (ν_3) asymmetric stretching fundamental, for ^{12}C and ^{13}C isotopologues (in natural abundance), respectively. Figure 5 shows the ($\nu_1 + \nu_3$) and ($2\nu_2 + \nu_3$) CO$_2$ combination bands.

The CO$_2$ bending fundamental (ν_2) has a double-peaked substructure at ~660/655 cm^{-1}. The high-frequency component is highly asymmetric with a long blue (high wavenumber) wing, while the low-frequency component is relatively symmetric. The ^{12}CO$_2$ asymmetric stretching fundamental (ν_3) is located at ~2345 cm^{-1} (4.26 μm), and is redshifted from the gas-phase value at 2348 cm^{-1} due to interactions with the surrounding matrix environment. The profile is asymmetric with a prominent blue shoulder and a weaker red (low wavenumber) shoulder. The asymmetric stretching fundamental (ν_3) of the ^{13}CO$_2$ isotopologue is found in its natural abundance

at ~2283 cm^{-1} (4.38 μm), similarly redshifted from its gas-phase value. The ^{13}CO$_2$ (ν_3) feature also exhibits shoulders on both sides (Fig. 4). The CO$_2$ (ν_1) symmetric stretching fundamental at ~1385 cm^{-1} (7.22 μm) is IR inactive (Falk & Seto 1986). The CO$_2$ ($\nu_1 + \nu_3$) combination band and ($2\nu_2 + \nu_3$) combination/overtone bands appear at ~3708 cm^{-1} (2.70 μm) and 3599 cm^{-1} (2.78 μm), respectively. The combination modes have narrow, relatively symmetric profiles. These bands are close to the broad H$_2$O stretching mode around 3300 cm^{-1} (3.03 μm) which typically dominates the observational ice spectra. However, unlike the strong ν_2 and ν_3 modes, the CO$_2$ combination and the ^{13}CO$_2$ (ν_3) modes are weak and unaffected by grain shape effects. Thus, their band shape profiles depend only on the chemical composition of interstellar CO$_2$ ice (e.g., Keane et al. 2001).
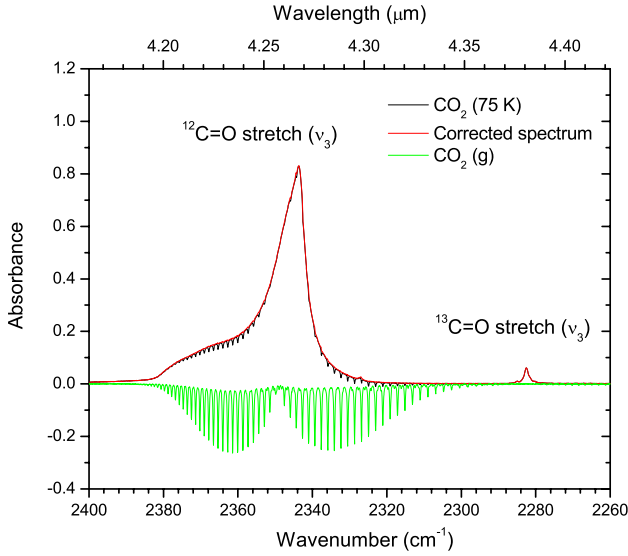
Fig. 6. Spectral corrections performed on the CO_2 (ν_3) mode. Rotational fine-structure of gaseous CO_2 (green trace), overlapping with the CO_2 (ν_3) ice band, is subtracted from the raw spectrum (black trace). The corrected spectrum is shown in red.

Table 1. High-resolution (0.1 cm^{-1}) band positions ($\tilde{\nu}$) and linewidths (FWHM) in pure CO_2 ice.

T (K)	$\tilde{\nu}$ (cm^{-1})	$FWHM$ (cm^{-1})	$\tilde{\nu}$ (cm^{-1})	$FWHM$ (cm^{-1})
	CO$_2$ bend (ν_2)			
15	659.72	5.12	654.53	2.09
30	659.78	4.35	654.53	2.00
45	659.72	3.64	654.53	1.86
60	659.78	2.81	654.59	1.48
75	659.72	2.31	654.65	1.17
	^{12}CO$_2$ stretch (ν_3)		^{13}CO$_2$ stretch (ν_3)	
15	2344.41	13.39	2282.76	1.94
30	2344.41	12.88	2282.70	1.91
45	2344.35	11.94	2282.58	1.83
60	2343.81	10.57	2282.58	1.55
75	2343.69	9.23	2282.52	1.38
	CO$_2$ comb. ($\nu_1 + \nu_3$)		CO$_2$ comb. ($2\nu_2 + \nu_3$)	
15	3708.02	1.92	3599.48	1.17
30	3708.02	1.91	3599.48	1.21
45	3707.90	1.73	3599.48	1.09
60	3707.84	1.32	3599.48	0.89
75	3707.78	1.10	3599.54	0.74

3.1. Corrections

In the laboratory, the CO_2 ice feature around 2350 cm^{-1} is easily contaminated with absorptions of gaseous CO_2 along the IR beam path. Variable concentrations relative to the background spectrum may cause under- or over-subtraction of interfering rotational lines. Same is true for the CO_2 bending mode around 660 cm^{-1} where an absorption band is seen around 668 cm^{-1}. The spectra are corrected using a gaseous CO_2 spectrum extracted from the background spectrum (Fig. 6). The bending mode region also suffers from spectral artifacts due to being located in the edge of the spectrometer spectral range. The (ν_2) bands presented here are therefore smoothed by superposition of several Gaussians. All spectra have been baseline corrected, and are available in reduced as well as in raw format in the Leiden ice database[2].

4. Discussion

Table 1 lists the band positions and bandwidths of pure CO_2 ice features for the five different temperatures in the 0.1 cm^{-1} resolution spectra. The values are obtained by the integration procedure in the Origin 7.5 software package. Figure 7 visualizes the derived values, including relative peak intensity and integrated area, as a function of temperature, together with other values available from the literature. The values are normalized to those in the 0.1 cm^{-1} spectra at 15 K. The influence of thermal annealing on the peak position depends on the influence of the trapping site on the specific vibrational mode. In general, all CO_2 band widths decrease at elevated temperatures. The narrowing is gradual and is observed already between 15 and 30 K. During the thermal annealing process, molecules rearrange themselves by finding energetically more favorable orientations. As the range of environments is reduced, the band profiles become more narrow. Simultaneously, the peak intensities

increase. The integrated area of all features peaks around 40 K, after which it declines until the ice desorbs between 80 and 90 K.

Comparison of the peak positions in the high-resolution spectra with those from lower resolution studies (Sandford & Allamandola 1990; Ehrenfreund et al. 1997; van Broekhuizen et al. 2006) generally shows agreement within the limitations due to resolution, assuming that at 1 cm^{-1} resolution, the error in position is 0.5 cm^{-1}. At 15 K, the CO_2 (ν_2) bending mode peaks at 659.7 and 654.5 cm^{-1}. The low-wavenumber component shifts by 0.12 cm^{-1} between 45 and 75 K. The observed shift is below the resolution of previous studies. The high-wavenumber component does not shift with temperature. The CO_2 (ν_3) stretching mode, peaking at 2344.4 cm^{-1} in the 15 K spectrum, red-shifts by 0.7 cm^{-1} for temperatures between 30 and 75 K. The $^{13}CO_2$ stretching mode undergoes a smaller (0.3 cm^{-1}) red-shift in a similar temperature range. The peak positions derived for the combination modes ($\nu_1 + \nu_3$) and ($2\nu_2 + \nu_3$) at 15 K are 3708.0 and 3599.5 cm^{-1}. The position of the combination modes shifts <0.25 cm^{-1} between 15 and 75 K. The shift of the ($\nu_1 + \nu_3$) band occurs above 30 K, toward lower wavenumbers.

The main objective of this high-resolution study is to fully resolve the Davydov splitting in the CO_2 (ν_2) bending mode. Figure 8 shows the dip-to-peak ratio, defined by Zasowski et al. (2009) as the local minimum to local maximum ratio of the blue peak, for 0.1 and 1.0 cm^{-1} resolution spectra as a function of temperature. For the high-resolution CO_2 ice feature, the dip-to-peak ratio decreases from 0.3 to <0.10 between 15 and 75 K. The ratio derived from the lower resolution spectra (Ehrenfreund et al. 1997) is ~20 % larger for all studied temperatures. A smaller dip-to-peak ratio confirms that the CO_2 bending mode and in particular the Davydov split is better resolved in the 0.1 cm^{-1} spectra.

The double peaked structure of the CO_2 bending mode is a diagnostic for the observed 15.2 μm CO_2 ice band. The interpretation of the CO_2 ice composition from observational spectra relies on laboratory spectra of CO_2 for different ice environments (Gerakines et al. 1999; Keane et al. 2001; Pontoppidan et al. 2008). The quality of the laboratory spectra therefore

---

[2] http://www.strw.leidenuniv.nl/lab/databases/co2_hires/
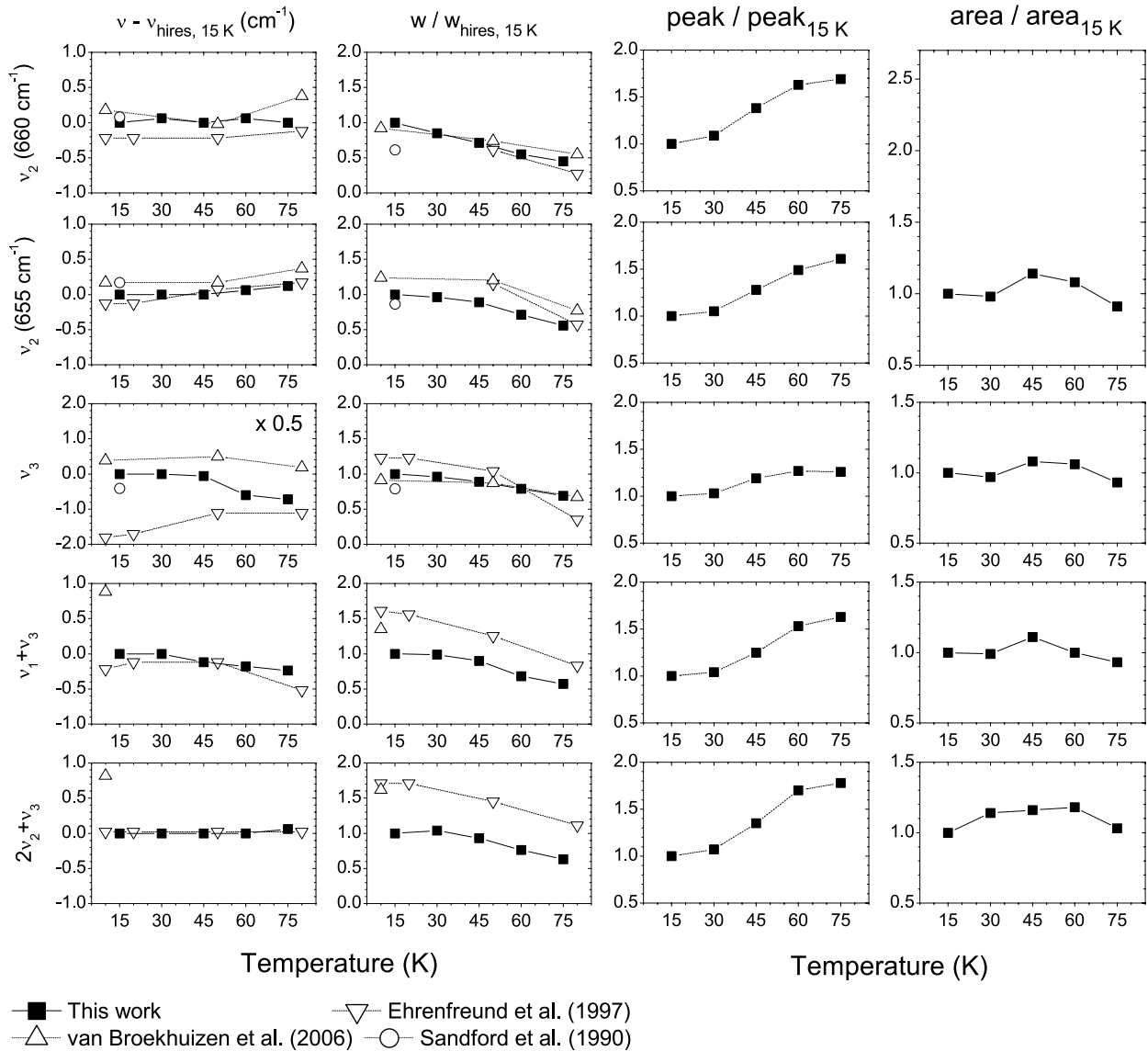
Fig. 7. Relative peak position (in cm^{-1}), width, peak intensity and integrated area of the CO_2 ice features with respect to the 15 K values as a function of temperature.
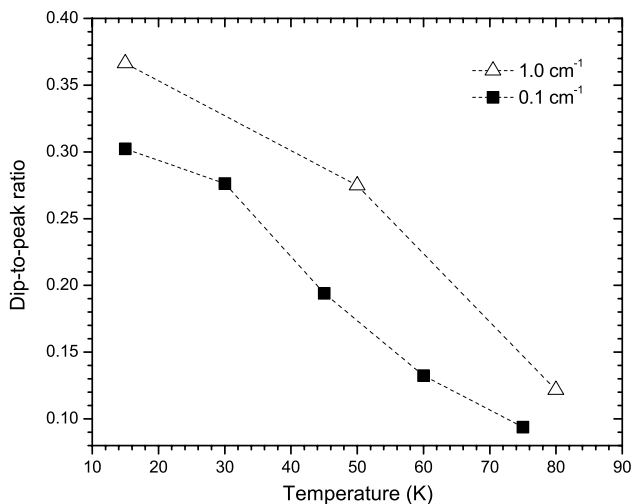
Fig. 8. Dip-to-peak ratio at different temperatures derived from the 0.1 cm^{-1} (filled squares) and 1.0 cm^{-1} (open triangles) resolution spectra of the CO_2 bending mode.

directly influences the derived ice composition from observations. Particularly for sources with larger contributions from pure CO_2 ice, a properly resolved Davydov splitting is a prerequisite for an accurate interpretation. Thus, the incorporation of 0.1 cm^{-1} resolution laboratory spectra (Table 1) into the fitting procedure is expected to improve the interpretation of the astronomical observations.

5. Summary

In this work we provide highly resolved (0.1 cm^{-1}) IR spectra of pure CO_2 ice at a spectral range of 4000–400 cm^{-1}, at temperatures 15, 30, 45, 60, 75 K. The spectral range covers the fundamental bending mode (ν_2), antisymmetric $^{12}CO_2$ and $^{13}CO_2$ stretching modes (ν_3) and the CO_2 combination mode ($\nu_1 + \nu_3$) and combination/overtone mode ($2\nu_2 + \nu_3$). The improved spectral parameters are needed for a more accurate interpretation of astronomical ice data. Moreover, the high spectral resolution allows an accurate quantification of thermally induced changes in CO_2 band profiles that are below the resolution of

previous work. This is particularly true for shifts in line position below 0.5 cm^{-1}. Also, the Davydov splitting in the ν_2 band is characterized more accurately and allows a better interpretation of astronomical spectra along lines of sight with thermally processed ices, where segregation and/or distillation causes CO_2 to be present in pure form as well. All data are available in the Leiden ice database[3].

References

Baratta, G. A., & Palumbo, M. E. 1998, J. Opt. Soc. Am. A, 15, 3076
Bergin, E. A., Langer, W. D., & Goldsmith, P. F. 1995, ApJ, 441, 222
Bergin, E. A., Melnick, G. J., Gerakines, P. A., Neufeld, D. A., & Whittet, D. C. B. 2005, ApJ, 627, L33
Boogert, A. C. A., Ehrenfreund, P., Gerakines, P. A., et al. 2000, A&A, 353, 349
Boogert, A. C. A., Pontoppidan, K. M., Lahuis, F., et al. 2004, ApJS, 154, 359
Boonman, A. M. S., van Dishoeck, E. F., Lahuis, F., & Doty, S. D. 2003, A&A, 399, 1063
Cook, A. M., Whittet, D. C. B., Shenoy, S. S., et al. 2011, ApJ, 730, 124
Cruikshank, D. P., Meyer, A. W., Brown, R. H., et al. 2010, Icarus, 206, 561
Cuppen, H. M., Penteado, E. M., Isokoski, K., van der Marel, N., & Linnartz, H. 2011, MNRAS, 417, 2809
Davydov, A. 1962, Nucl. Phys. A, 37, 106
d'Hendecourt, L. B., & Jourdain de Muizon, M. 1989, A&A, 223, L5
Ehrenfreund, P., Boogert, A. C. A., Gerakines, P. A., Tielens, A. G. G. M., & van Dishoeck, E. F. 1997, A&A, 328, 649
Ehrenfreund, P., Dartois, E., Demyk, K., & D'Hendecourt, L. 1998, A&A, 339, L17
Ehrenfreund, P., Kerkhof, O., Schutte, W. A., et al. 1999, A&A, 350, 240
Falk, M., & Seto, P. F. 1986, Can. J. Spectros., 31, 134
Fayolle, E. C., Öberg, K. I., Cuppen, H. M., Visser, R., & Linnartz, H. 2011, A&A, 529, A74
Fuchs, G. W., Cuppen, H. M., Ioppolo, S., et al. 2009, A&A, 505, 629
Fulvio, D., Raut, U., & Baragiola, R. A. 2012, ApJ, 752, L33
Gerakines, P. A., Schutte, W. A., Greenberg, J. M., & van Dishoeck, E. F. 1995, A&A, 296, 810
Gerakines, P. A., Schutte, W. A., & Ehrenfreund, P. 1996, A&A, 312, 289
Gerakines, P. A., Whittet, D. C. B., Ehrenfreund, P., et al. 1999, ApJ, 522, 357
Gomis, O., & Strazzulla, G. 2005, Icarus, 177, 570
Goumans, T. P. M., & Andersson, S. 2010, MNRAS, 406, 2213
Hudgins, D. M., Sandford, S. A., Allamandola, L. J., & Tielens, A. G. G. M. 1993, ApJS, 86, 713

Ioppolo, S., Palumbo, M. E., Baratta, G. A., & Mennella, V. 2009, A&A, 493, 1017
Ioppolo, S., van Boheemen, Y., Cuppen, H. M., van Dishoeck, E. F., & Linnartz, H. 2011, MNRAS, 413, 2281
Jamieson, C. S., Mebel, A. M., & Kaiser, R. I. 2006, ApJS, 163, 184
Keane, J. V., Boogert, A. C. A., Tielens, A. G. G. M., Ehrenfreund, P., & Schutte, W. A. 2001, A&A, 375, L43
Knez, C., Boogert, A. C. A., Pontoppidan, K. M., et al. 2005, ApJ, 635, L145
Loeffler, M. J., Baratta, G. A., Palumbo, M. E., Strazzulla, G., & Baragiola, R. A. 2005, A&A, 435, 587
Madzunkov, S., Shortt, B. J., Macaskill, J. A., Darrach, M. R., & Chutjian, A. 2006, Phys. Rev. A, 73, 020901
Mennella, V., Palumbo, M. E., & Baratta, G. A. 2004, ApJ, 615, 1073
Mennella, V., Baratta, G. A., Palumbo, M. E., & Bergin, E. A. 2006, ApJ, 643, 923
Moore, M. H., Khanna, R., & Donn, B. 1991, J. Geophys. Res., 96, 17541
Nummelin, A., Whittet, D. C. B., Gibb, E. L., Gerakines, P. A., & Chiar, J. E. 2001, ApJ, 558, 185
Öberg, K. I., Fayolle, E. C., Cuppen, H. M., van Dishoeck, E. F., & Linnartz, H. 2009, A&A, 505, 183
Palumbo, M. E., Baratta, G. A., Brucato, J. R., et al. 1998, A&A, 334, 247
Pontoppidan, K. M., Fraser, H. J., Dartois, E., et al. 2003, A&A, 408, 981
Pontoppidan, K. M., Boogert, A. C. A., Fraser, H. J., et al. 2008, ApJ, 678, 1005
Poteet, C. A., Megeath, S. T., Watson, D. M., et al. 2011, ApJ, 733, L32
Poteet, C. A., Pontoppidan, K. M., Megeath, S. T., et al. 2013, ApJ, 766, 117
Raut, U., & Baragiola, R. A. 2011, ApJ, 737, L14
Roser, J. E., Vidali, G., Manicò, G., & Pirronello, V. 2001, ApJ, 555, L61
Sandford, S. A., & Allamandola, L. J. 1990, ApJ, 355, 357
Satorre, M. A., Palumbo, M. E., & Strazzulla, G. 2000, Ap&SS, 274, 643
Slanger, T. G., Wood, B. J., & Black, G. 1972, J. Chem. Phys., 57, 233
Talbi, D., Chandler, G. S., & Rohl, A. L. 2006, Chem. Phys., 320, 214
Tielens, A. G. G. M. & Hagen, W. 1982, A&A, 114, 245
Tso, T., & Lee, E. 1985, J. Phys. Chem., 89, 1612
van Broekhuizen, F. A., Groot, I. M. N., Fraser, H. J., van Dishoeck, E. F., & Schlemmer, S. 2006, A&A, 451, 723
van Dishoeck, E. F., Helmich, F. P., de Graauw, T., et al. 1996, A&A, 315, L349
Watanabe, N., & Kouchi, A. 2002, ApJ, 567, 651
Watanabe, N., Nagaoka, A., Shiraki, T., & Kouchi, A. 2004, ApJ, 616, 638
Watanabe, N., Nagaoka, A., Hidaka, H., et al. 2006, Planet. Space Sci., 54, 1107
White, D. W., Gerakines, P. A., Cook, A. M., & Whittet, D. C. B. 2009, ApJS, 180, 182
White, D. W., Mastrapa, R. M. E., & Sandford, S. A. 2012, Icarus, 221, 1032
Whittet, D. C. B., Gerakines, P. A., Tielens, A. G. G. M., et al. 1998, ApJ, 498, L159
Whittet, D. C. B., Shenoy, S. S., Bergin, E. A., et al. 2007, ApJ, 655, 332
Whittet, D. C. B., Cook, A. M., Chiar, J. E., et al. 2009, ApJ, 695, 94
Zasowski, G., Kemper, F., Watson, D. M., et al. 2009, ApJ, 694, 459

---

[3] http://www.strw.leidenuniv.nl/lab/databases/co2_hires/